



Highly-efficient isolation of microcrystalline cellulose and nanocellulose from sunflower seed waste via environmentally benign method

Kydyrmolla Akatan · Sana Kabdrakhmanova ·
Tilek Kuanyshbekov · Zhanar Ibraeva ·
Ainur Battalova · K. S. Joshy · Sabu Thomas

Received: 5 August 2021 / Accepted: 7 March 2022 / Published online: 29 March 2022
© The Author(s), under exclusive licence to Springer Nature B.V. 2022

Abstract The main focus of the study was to create natural microcrystalline cellulose obtained from a raw material source, the residue of sunflower seeds following oil extraction. For this purpose, organosolvent oxidation was chosen instead of the conventional method, whereby microcrystalline cellulose (MCC) was extracted from sunflower seed husks (SFHs), after which the refining of cellulose nanocrystals (CNCs) was carefully conducted. The organosolvent method of obtaining MCC involves

the use of peroxyacetic acid (PAA), which provides a high yield of cellulose and eliminates the need to use chlorine-containing compounds in the process of bleaching. The environmentally benign method of obtaining MCC using the organosolvent method consisted of halving the concentration of acetic acid and hydrogen peroxide, to 58% and 15%, respectively, so as to obtain PAA, which yields an MCC of 47.8%. Physico-chemical characterization of particle sizes, optical properties, chemical and crystal structure, surface morphology, and thermal stability of MCC and CNCs was performed. FTIR analysis revealed the structural similarity of all the materials of the extracted cellulose. Surface morphology was observed using SEM, showing that the surface of MCC fibers appeared rough, whereas that of CNCs was smooth with overlapping rod-like structures. The surface of CNC film was found to be colorless and composed of nanofibrils. XRD analysis and determination of average particle size revealed that the MCC had a crystallinity index (CI) of $72.9 \pm 4\%$, a coherent scattering length (CSL) of 2.9 ± 0.1 nm, and an average particle length of 1971 ± 100 nm and width of 266 ± 35 nm. Acid hydrolysis resulted in the reduction of the length of CNCs by 4 times and the width by around 5 times, accompanied by an increase in the CI value. Cellulose was found to break down in the temperature range of 200–358 °C. Overall, SFHs are considered to be an effective potential source for CNCs, while the method employed herein for the extraction of cellulose from agricultural biomass waste is both cost-effective and environmentally benign.

K. Akatan · T. Kuanyshbekov · A. Battalova
Amanzholov University, 55 Kazakhstan str.,
Ust-Kamenogorsk, Kazakhstan

K. Akatan · S. Kabdrakhmanova (✉) · T. Kuanyshbekov ·
Z. Ibraeva · A. Battalova
Scientific Center of Composite Materials, 79 Nurmakov
str., Almaty, Kazakhstan
e-mail: sanaly33@mail.ru

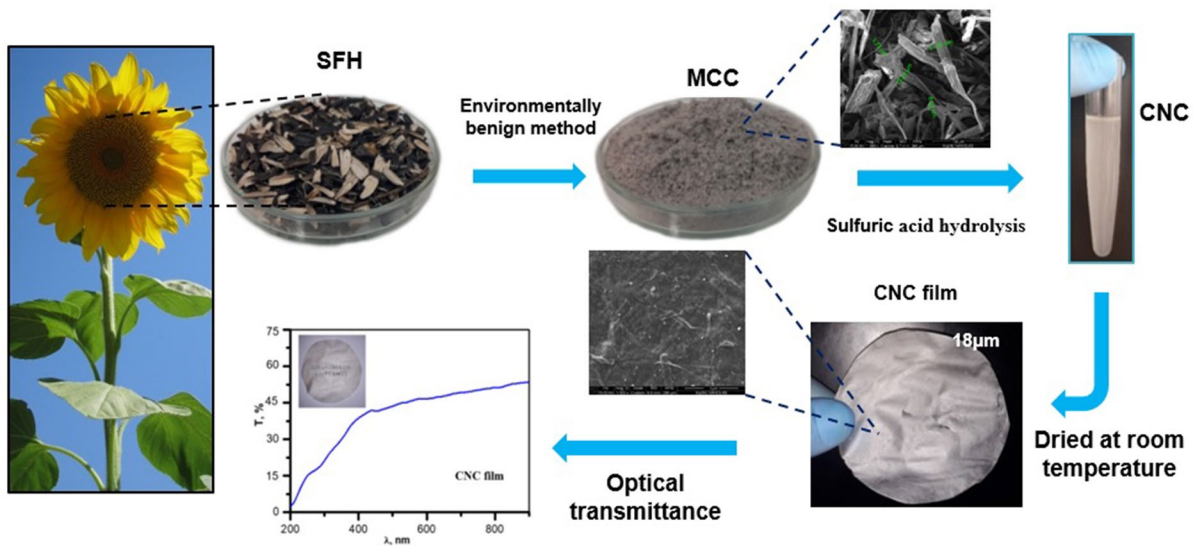
S. Kabdrakhmanova
Satbayev University, 22, Satbayev str., Almaty, Kazakhstan

Z. Ibraeva
Abai Kazakh National Pedagogical University, 13
Dostykave., Almaty, Kazakhstan

K. S. Joshy
Department of Mechanical and Industrial Engineering,
College of Engineering, Qatar University, 2713, Doha,
Qatar

K. S. Joshy · S. Thomas
School of Energy Materials, Mahatma Gandhi University,
Kottayam, Kerala 686560, India

Graphical abstract



Keywords Sunflower husks · Organosolvent oxidation · Microcrystalline cellulose · Cellulose nanocrystals

Introduction

Currently, cellulosic materials are widely used in various industries, due to their abundance, biocompatibility and biodegradability (Alves et al. 2015; Alemdar et al. 2008; Hamawand et al. 2020). Hence, the production of microcrystalline cellulose and nanocellulose from various sources has garnered much attention in both scientific and industrial sectors. This is primarily due to their mechanical and thermal properties, as well as cost-effectiveness and versatility (Sá et al. 2015; Rambabu et al. 2016). The extremely ordered structure of CNCs ensures their high strength, which preconditions their use as a component in reinforcing systems (Kvien et al. 2005; Oksman et al. 2006; Bondeson et al. 2006). In addition, the application of CNCs as a filler in polymeric materials improves the mechanical properties of said materials and helps to control humidity, optical and sorption properties, and biodegradability (Belén et al. 2017; Abdul Khalil et al. 2014).

Additionally, the CNC suspension can self-assemble to form left-handed chiral liquid crystals as it reaches critical concentration (Gray 2016; Sun et al. 2019), the helix structure of which can be maintained in the dried film through the slow evaporation of water (Edgar et al. 2001). As a result, the solid CNC film exhibits unique optical properties. Moreover, the presence of incident light wavelengths in the visible range causes the material to appear colorful to the naked eye (Blaise et al. 2017). To date, research on this optical film has aroused far-ranging interest, such as in the fields of optical anti-counterfeiting, sensors, and composite devices (Lin et al. 2019; Kim et al. 2020). This has led to the application of CNC film in the pharmaceutical, food, electronic and chemical industries.

Plant-based materials are the main sources of cellulosic components, which include annual plants, agricultural wastes, bacteria and molds (Brown et al. 2000; Boerjan et al. 2003). Materials rich in cellulose, hemicelluloses and lignin are commonly referred to as lignocellulosic biomass (Carrier et al. 2011). Wastes such as straw, the husks of rice and corn, sugarcane pulp, nypafrutican stems, the fibers of pineapple and banana leaves, and coconut shells are typical sources of lignocellulosic biomass (Boerjan et al.

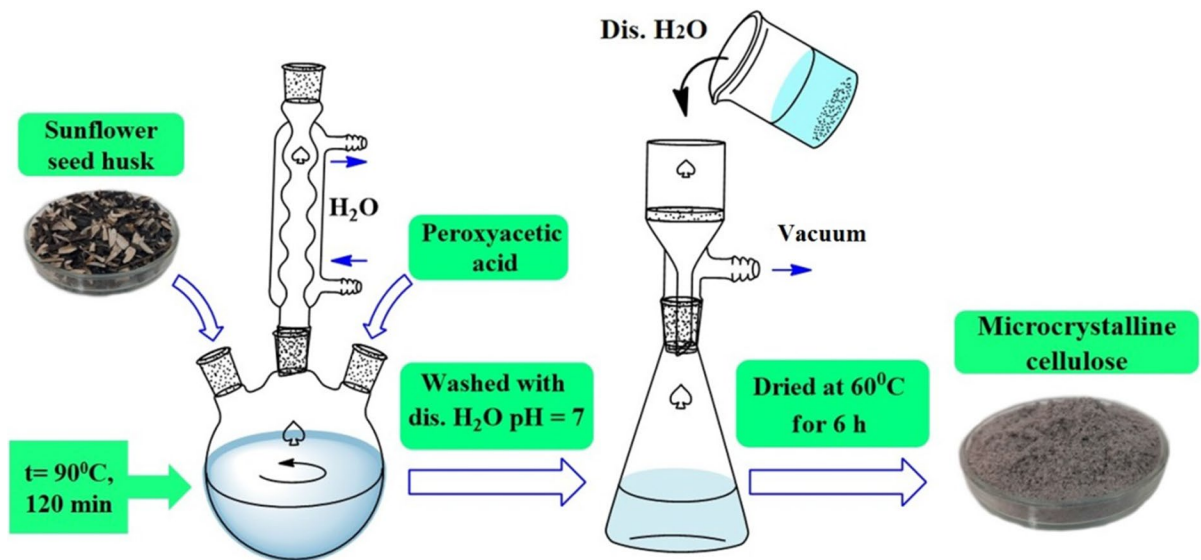


Fig. 1 Diagram representing the synthesis of MCC via organosolvent oxidation

2003; Gibson et al. 2010; Lwako et al. 2013; Sumira et al. 2020; Song et al. 2009; Chen et al. 2015; Jayaraj et al. 2014; An et al. 2020).

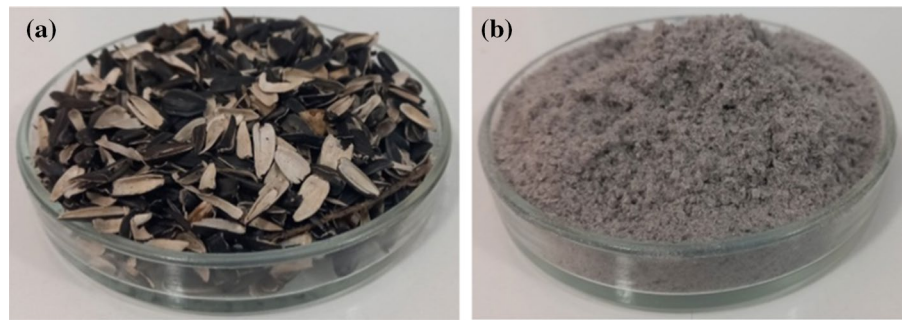
Kazakhstan has an urgent need for the replacement of cellulose from trees as a raw material used in the production of paper, which would be an excellent application of lignocellulosic biomass from agricultural waste. Further, agriculture is an important part of the economy of Kazakhstan, and generates large quantities of waste every year, which is mostly neither reused nor recycled.

An important source of lignocellulose biomass is SFH, which is a by-product from the preparation of sunflower seeds for oil extraction, forming about 14% of the total seed volume of sunflower seeds of Kazakhstani production. SFH is a lignified plant tissue of cylindrical shape of up to 20–70 mm in length and approximately 8 mm in diameter, having a density of up to 1.2 thousand kg per cubic meter and a humidity level of up to 8%. According to some studies, the cellulose content in SFH is 31–42.4% of the total mass (Ovcharov et al. 2010; Khusid et al. 2015).

Sunflower farming is one of the leading branches of agriculture in Kazakhstan, and the area under cultivation for the purpose of oil extraction has been growing steadily, now exceeding one million hectares,

which amounts to around 5% of all agricultural land in the country. Due to the high demand for sunflower seeds, their processing generates huge amounts of waste, the disposal of which in large quantity is both expensive and complicated. The method utilized in oil extraction is known to produce approximately 14–25 kg of husks from every 100 kg of sunflower seeds (Harkov et al. 2018). Moreover, the use of SFHs in their pure form as animal feed is undesirable, due to the high content of fiber, being approximately 50%, because it is poorly absorbed in the gastrointestinal tract (Khusid et al. 2015). Hence, the processing of large amounts of SFHs is a serious problem that needs to be resolved immediately, as much of said waste is simply burned as fuel.

There are a number of studies that have been carried out on the production of nanocellulose from agricultural waste (Boerjan et al. 2003; Gibson et al. 2010; Song et al. 2009; An et al. 2020; Bongao et al. 2020; Israel et al. 2008; Yandan et al. 2015). In addition to rice, straw and the aforementioned husks (Boerjan et al. 2003; Gibson et al. 2010; Lwako et al. 2013; Sumira et al. 2020), attention has been paid to the residue of coniferous wood, inclusive of wood chips, pine branches and needles, with a target production yield of more than 13% (Rosana et al. 2016;

Fig. 2 a Raw SFHs and b MCC

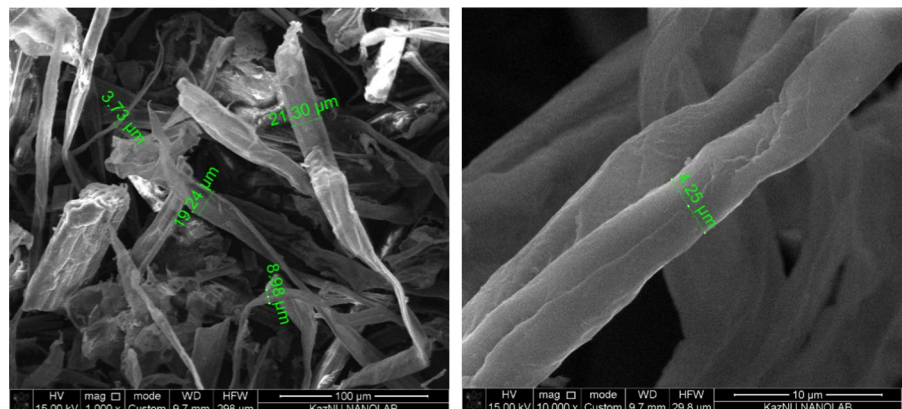
Kunaver et al. 2016). Furthermore, among the plants that could be cultivated in Kazakhstan, special consideration should be given to hemp, with a cellulose content in the plant stems that exceeds 50–70% (Jean et al. 2010). Analysis of the applicable literature shows that there are few studies related to the processing of SFHs into nanocellulose. Nevertheless,

SFHs have been studied with regards to their use as functional animal feed additives (Khusid et al. 2015), carbon adsorbents for the removal of oil from water (Ovcharov et al. 2010), fuel (Perea-Moreno et al. 2018; Zajemska et al. 2017), fertilizers (Dmytro et al. 2021), biosorbent for the extraction of metals (Saleh et al. 2016; Tomasz et al. 2021), and agar medium

Table 1 Effect of SFH:PAA ratio on MCC quality.

SFH:PAA, g/mL	Quality indicators of MCC					
	Yield, %	Humidity, %	β -Cellulose, %	Residual lignin, %	Hemicellulose, %	Ash content (SiO ₂), %
1:8	32.9±2	2.7±0.5	49±3	3.6±0.5	21.2±2	2.4±0.5
1:10	32.6±2	2.8±0.5	53.4±3	3.2±0.5	18.1±2	2.4±0.5
1:12	32.8±2	2.8±0.5	53.4±3	3.1±0.5	15.8±2	2.3±0.5
1:14	32.7±2	2.7±0.5	62.3±3	2.8±0.5	14.5±2	2.5±0.5
1:16	36.5±2	2.9±0.5	66.6±3	2.6±0.5	13.94±2	2.2±0.5
1:18	44±2	2.7±0.5	68.8±3	2.4±0.5	13.7±2	2.2±0.5
1:20	47.8±2	2.7±0.5	72±3	2.1±0.5	13.02±2	2.2±0.5
1:22	47.83±2	2.7±0.5	72±3	2.1±0.5	13.02±2	2.2±0.5
1:24	47.84±2	2.7±0.5	72±3	2.1±0.5	13.02±2	2.1±0.5

The ratio of SFH:PAA 1:20 g/mL is considered the most effective for obtaining MCC, therefore bold indicates Quality of MCC

Fig. 3 SEM images of MCC

(Khan et al. 2005), as well as the manufacture of ceramics from SFH ash (Quaranta et al. 2016). One of the few studies devoted to the production of nanocellulose using SFHs involved pretreatment with sodium hydroxide, bleaching with sodium hypochlorite, ethanol precipitation, acid hydrolysis with sulfuric acid, and finally dialysis in order to obtain nanocellulose (Chen et al. 2015). Of note is that alkaline treatment and bleaching with sodium hypochlorite significantly increase the formation of liquid waste.

Therefore, in the pretreatment of biomass, the use of the environmentally friendly, one-step organosolvent oxidation method is best. This method does not require any additional bleaching process, as the chlorine-containing bleaching reagents produce cellulose material via a cyclic method using the existing peroxyacetic acid (PAA), which can be reused several times (Barbash et al. 2020). In studies, high-yield cellulose materials have been obtained from annual plants using PAA (Vurasko et al. 2014). However, the use of concentrated acetic acid and 30% hydrogen peroxide to produce PAA in this method clearly prevents it from being considered as a completely environmentally safe method. Further, no systematic studies on the extraction of MCC and nanocellulose from SFHs using green technology have been conducted.

Considering these factors, the main purpose of this study is to obtain MCC from SFHs using a more environmentally friendly method, as well as to establish the optimal value of the delignification agent. The present study continued onto the creation of CNCs using acid hydrolysis of MCC, followed by the production of CNC film.

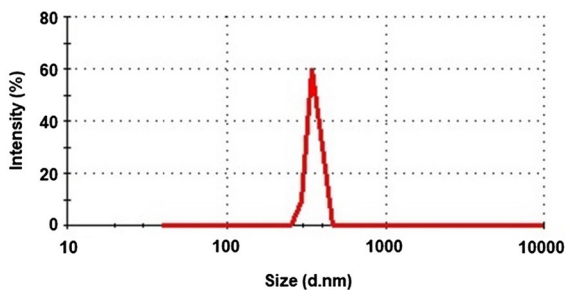


Fig. 4 The particle size of MCC

Experimental section

Materials

Hydrogen peroxide, H_2O_2 , 15%, acetic acid (CH_3COOH) $\geq 55\%$ and ethanol 96% (C_2H_5OH) were obtained from Alita LLP (Kazakhstan). Sulfuric acid (98% H_2SO_4), sodium hydroxide ($\geq 99\%$ NaOH), hexane (99% C_6H_{14}) were obtained from Sigma-Aldrich (Bangalore, India). SFHs were obtained from a local oil refinery (Sei-Nar LLP) located in Ust-Kamenogorsk, Kazakhstan. All other reagents were of analytical grade and were used without additional purification.

Methods

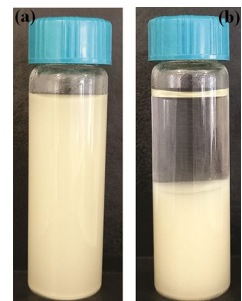
Sample preparation

SFHs were washed in hexane using a Soxhlet extractor for 2 h in order to eliminate unsaturated high fatty acids, such as stearic and palmitic acids, among others. The washed SFHs were placed in a drying cabinet at 50 °C for 6 h, until any hexane had completely evaporated.

Table 2 CI, CSL and average particle values of CNCs obtained from MCC via acid hydrolysis

Samples	CSL, nm	CI, %	Average particle size, nm	
			Length	Width
MCC	2.9 ± 0.1	72.9 ± 4	1971 ± 100	266 ± 35
CNC	2.7 ± 0.1	82 ± 4	450 ± 50	50 ± 15

Fig. 5 MCC suspension obtained from SFH. **a** fresh MCC and **b** after one month



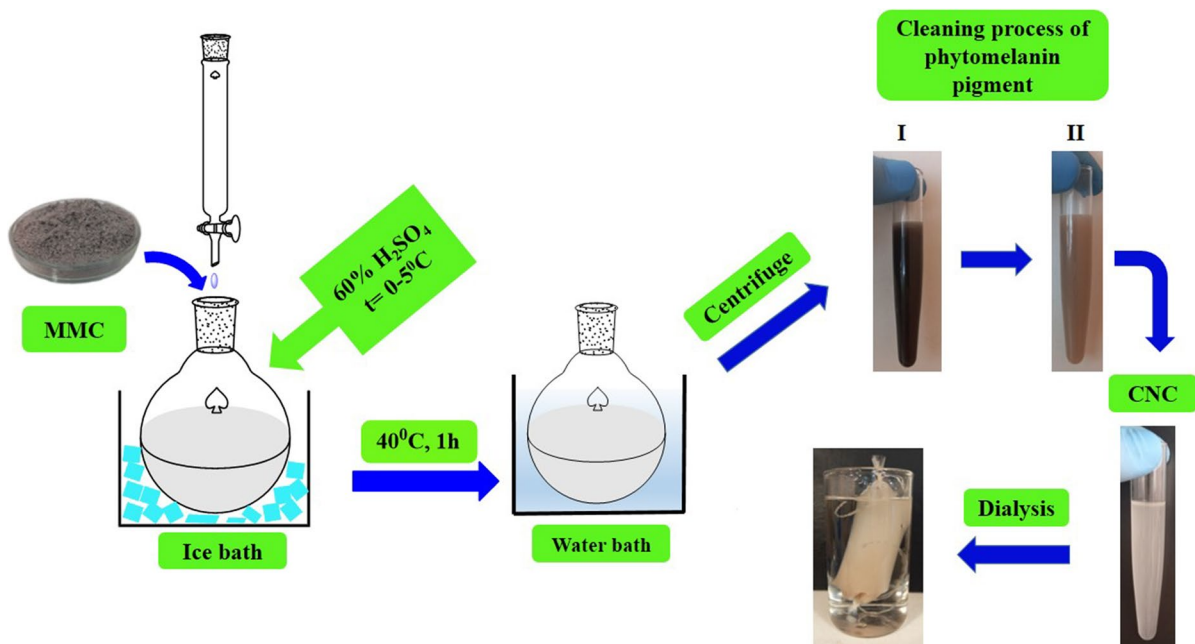
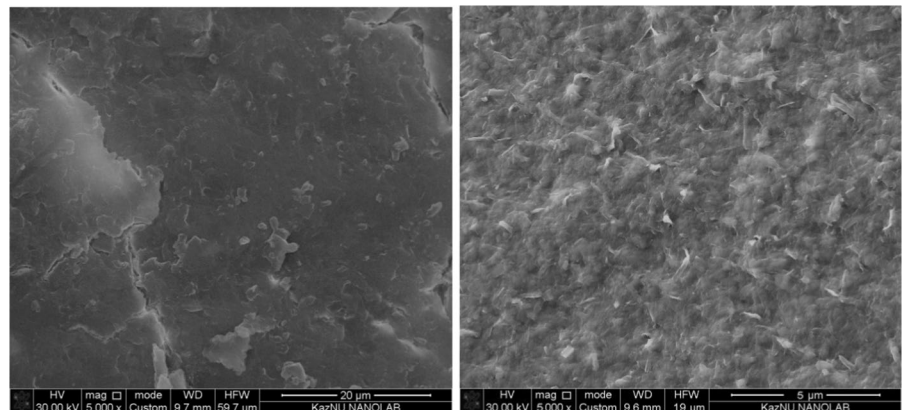


Fig. 6 Diagram of CNC synthesis via acid hydrolysis

Fig. 7 SEM image of CNCs



Preparation of peroxyacetic acid (PAA)

The detoxifying agent, PAA, was prepared in accordance with the method utilized by Vurasco et al. (2014), using concentrated sulfuric acid as a catalyst in a ratio of 1.5:1 (V_{mL}/V_{mL}) to 55 wt% glacial acetic acid ($\rho = 0.5836 \text{ mg/cm}^3$), which was then combined with 15 wt% ($\rho = 1.055 \text{ mg/cm}^3$) hydrogen peroxide.

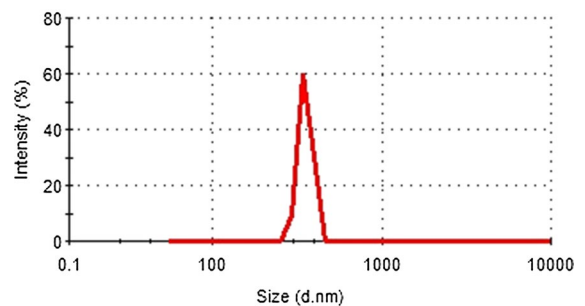


Fig. 8 The particle size of CNC

Fig. 9 CNC suspensions. **a** fresh CNC and **b** CNC after one month



Equilibrium peroxyacetic acid analysis

The concentration of PAA obtained was determined using the following formula:

$$C_{\text{PAA}} = V_1 N_1 \text{mEq} 100 / V_{\text{PAA}} 10 \rho \quad (1)$$

where V_1 is the volume of sodium thiosulfate used for sample titration (328 mL); N_1 is the normality of sodium thiosulfate concentration (0.1 N); mEq is the milliequivalent of PAA (0.038 mg/mol); V_{PAA} is the volume of the sample taken for titration (1 mL); and, ρ is the density of PAA (1.04 g/cm³) (Vurasco et. al 2014).

Extraction of microcrystalline cellulose (MCC)

In order to obtain MCC from SFH, an effective ratio of the raw material and the delignification agent had to be determined. MCC was obtained using 10 g of SFHs combined with PAA (g/mL) in the following ratios: 1/8, 1/10, 1/12, 1/14, 1/16, 1/18, 1/20, 1/22. Cellulose extraction was carried out by boiling the SFHs and PAA in a flask with a rotary condenser at 90 °C for 2 h, with continuous intensive magnetic

Fig. 10 CNC film production

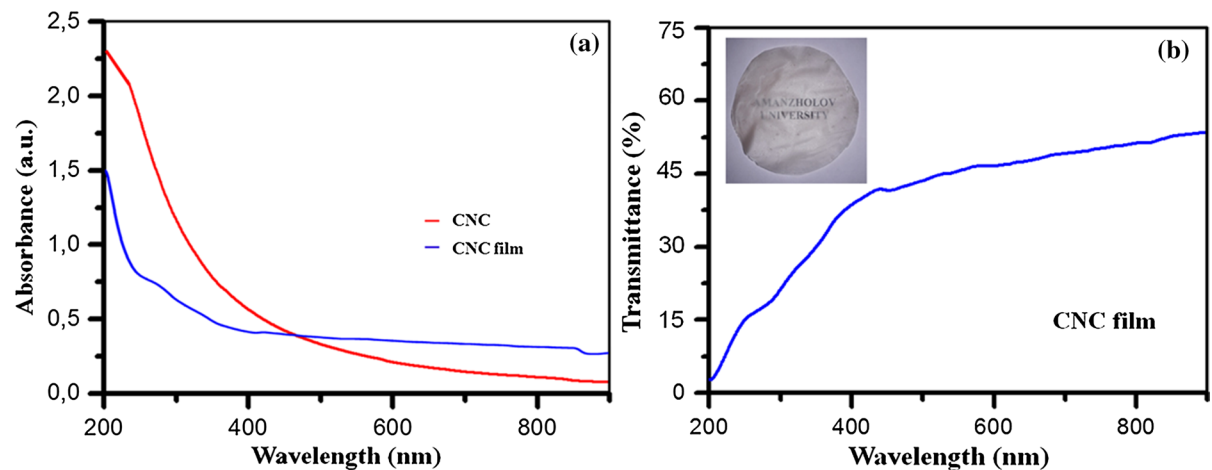
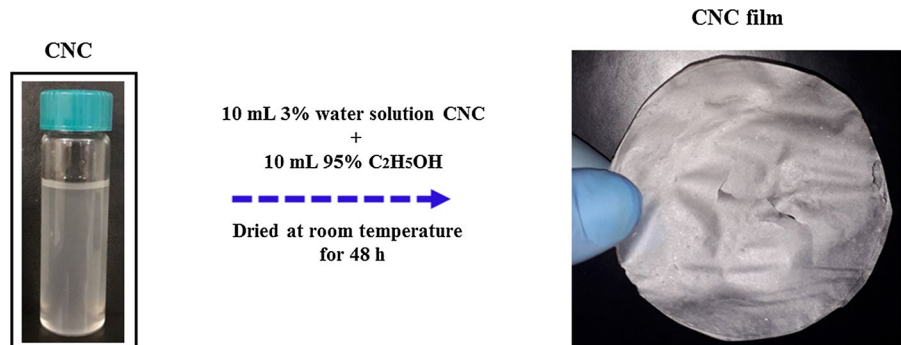


Fig. 11 **a** UV–vis spectrum of CNC and CNC film and **b** optical transmittance of CNC film

stirring (Fig. 1). The MCC obtained was cooled to 25 °C, run through filter paper, and finally neutralized by washing with distilled water until pH was equal to 7. The neutralized pulp was dried at 60 °C for 6 h, until the mass reached a stabilized consistency. The dried material was then stored in a desiccator.

Determination of MCC quality indicators

The moisture content of the fully dried MCC was determined by the ASTM D 1348–94 (2008) test protocol, β -cellulose content by ASTM D 588 (2000), residual lignin by ISO/DIS 21436, and hemicellulose content by ASTM D 5896–96 (2019) e1. In order to determine the ash content of cellulose (SiO_2), 3 g MCC was fired in a muffle furnace (SNOL 8.2/1100 L Lithuania) at 700 °C for 90 min. The mass of ash (SiO_2) was measured on an analytical balance (Sartogom LV 210-A, Russian) until an average value was obtained.

MCC yield was calculated using the following formula:

$$\text{Yield (\%)} = (m_{\text{SFH}} - m_{\text{MCC}}) / m_{\text{SFH}} \times 100\% \quad (2)$$

where m_{SFH} is SFH mass; and, m_{MCC} is the mass of the MCC obtained.

Sulfuric acid hydrolysis of nanocellulose

CNCs were obtained by way of acid hydrolysis of the resulting MCC using sulfuric acid (60 wt%) via the following procedure: 1 ± 0.01 g of the original MCC was weighed and gradually added into a sulfuric acid

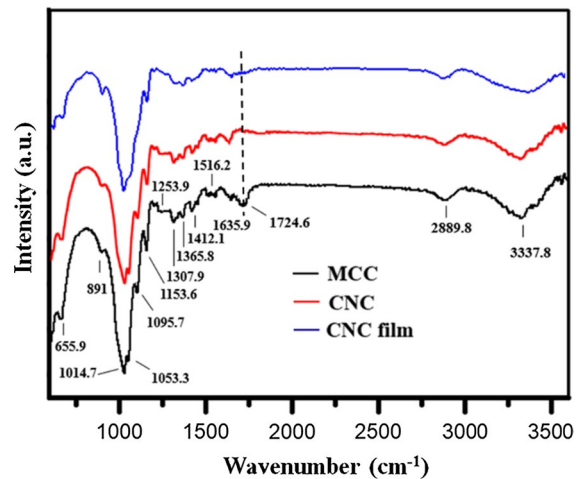
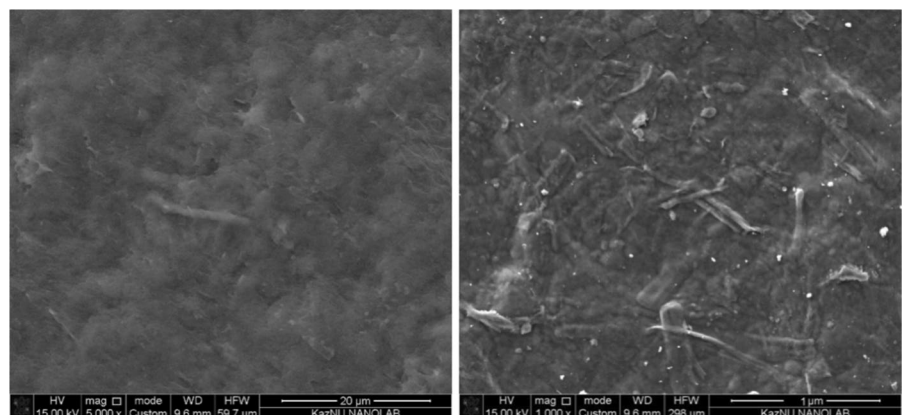


Fig. 13 FTIR spectra of MCC, CNCs and CNC film

solution at a ratio ($\text{MCC}:\text{H}_2\text{SO}_4$) of 1:8 g/mL and a temperature of 0–5 °C.

When the cellulose and acid were completely mixed and a gel-like mass was obtained, 25 mL of deionized water was added and then heated in a water bath at 40 ± 2 °C under mechanical stirring at 500 rpm for 1 h. CNC extraction from the resulting suspension consisted of two stages. In the first step, the CNCs were stripped of phytomelanin pigment. In order to do this, the suspension was centrifuged for 5 min at 1500 rpm/min (Centrifuge 5427R Eppendorf). As a result, the phytomelanin precipitated in the form of large black particles. The cleaning process was repeated 2 times until the large particles of pigment had been completely separated (Fig. 6).

Fig. 12 SEM images of CNC film



In the second stage of extraction, the CNCs were centrifuged at 8000 rpm for 15 min, followed by dialysis (Visking Dialysis Tubing MWCO-12–14,000 Daltons) for one week in deionized water until reaching a neutral pH. The CNC yield was calculated using the following formula:

$$\text{Yield (\%)} = (m_{\text{MCC}} - m_{\text{CNC}}) / m_{\text{MCC}} \times 100\% \quad (3)$$

where m_{MCC} is the mass of the MCC obtained by hydrolysis; and, m_{CNC} is the mass of the CNCs obtained after sulfuric acid hydrolysis.

The particle sizes and zeta potential of MCC and CNCs

A 2 wt% aqueous suspension of MCC and CNCs was subjected to 30 kHz for 10 min using an ultrasonic disperser, U-sonic UZTA-0.15/22–0 (Alena, Russian). The average particle size and zeta potential were determined via dynamic light scattering (DLS) using a Zetasizer NanoZS 90 (Malvern, UK). The measured electrophoretic mobility was then converted to the zeta potential.

Preparation of CNC film

In order to prepare the CNC film, 10 mL of 96% ethanol was added to 10 mL of an aqueous solution of 15 wt% CNCs, which was then stirred in a magnetic mixer for 15 min. The fully mixed solution was poured onto a flat plastic surface and dried at

25 ± 2 °C for 48 h. As a result, a colorless film with a thickness of 18 ± 1 μm formed. The samples were stored in a vacuum desiccator to prevent sorption of water vapor and carbon dioxide from the air.

FTIR spectroscopy

FTIR analysis of MCC, CNCs and CNC film were performed on an FT-801 FTIR spectrometer (Simex, Russian), with a resolution of 1 cm^{-1} at a range of $450\text{--}4700 \text{ cm}^{-1}$, in accordance with the standard method and using an accessory to measure attenuated total reflection (ATR) and specular-diffuse reflection (SDR), at a temperature of 25 ± 1 °C.

X-ray diffraction

The crystal structures of MCC, CNCs and CNC film were studied via X-ray diffraction on a X'PertPRO diffractometer (Malvern Panalytical Empyrean, Netherlands) using monochromatized copper ($\text{CuK}\alpha$) at a scan speed of 0.05° for 10 s, with a K-Alpha1 wavelength of 1.54187 \AA . Measurement in reflection mode, using an aluminium rectangular multi-purpose sample holder (PW1172/01), was performed at a diffraction angle 2θ between 10° and 40° , with the X-ray tube voltage at 45 kV, current intensity at 30 mA, and a measurement time of each step of 0.5 s. The ICDD PDF-4/AXIOM database of XRD pattern was used for the analysis of the resultant XRD patterns. The POWDER CELL 2.5 software package was used for

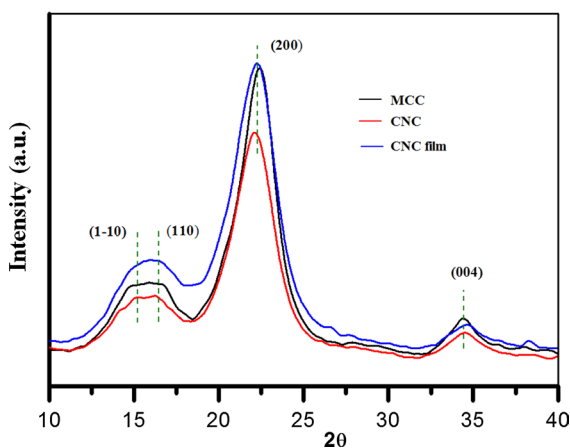


Fig. 14 XRD diffractions of MCC and CNCs and CNC film

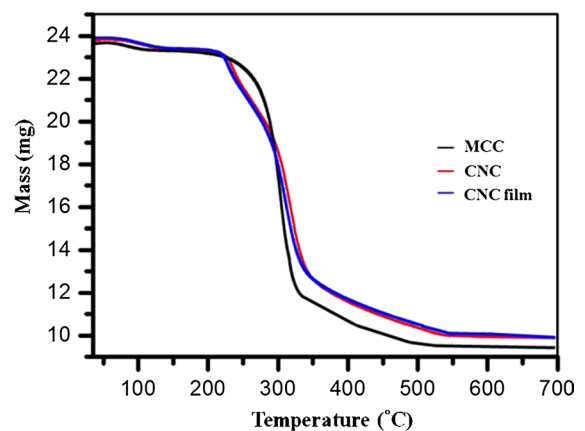


Fig. 15 TGA curves of MCC, CNCs and CNC film

the Rietveld refinement of the unit cell parameters and CSL, run 3 times using formula 4.

The crystallinity index was calculated using the following equation (Ling et al. 2019):

$$CI (\%) = \left(A_{\text{cryst}} / A_{\text{cryst}} + A_{\text{amorph}} \right) * 100\% \quad (4)$$

where A_{cryst} is the area under the calculated pattern for crystalline cellulose; and, A_{amorph} is the area under the pattern calculated for the amorphous content.

CSL was determined via the Scherrer formula:

$$CSL = k\lambda / \beta \cos\theta \quad (5)$$

where k is a shape factor that is often 0.89 (Sintu et al. 2019); λ is the wavelength of the diffractometer (0.1542 nm); β is the FWHM (maximum half of the full width) of the (200) diffraction peak in radians; and, θ is the diffraction angle.

UV-vis analysis of CNC and CNC film

The optical absorption spectrum of the CNC aqueous solution obtained was recorded on a spectrophotometer (PE-5400UV, Russian) with a scanning speed of 240 nm/min and a wavelength of 190–1000 nm. A 10 mm thick quartz cuvette was used. The transparency of the CNC film in the optical absorption region of 600 nm was calculated using the following formula:

$$\text{Opacity} = \text{Abs}_{600} / d \quad (6)$$

where Abs_{600} is the optical density of the CNC film of 600 nm; and, d is the thickness of the CNC film (μm).

Scanning electron microscopy

The surface morphologies of MCC, CNCs and CNC film were examined using a Quanta 200i 3D SEM (FEITM Netherlands). Measurements were carried out in high vacuum mode using a secondary electron detector at an accelerating voltage of 15 kV. 1 g of MCC and 1 g of CNC powders were each added into separate 50 mL solutions of deionized water and silver nanoparticles at a concentration of 10^{-3} mol/L and then mechanically stirred for 2 h. The prepared samples were run through filter paper and dried in

an oven at 50 ± 2 °C for 1 h. The surface of the CNC film was coated with gold nanoparticles to improve the transfer of electrons. Finally, the specimens were mounted on aluminum pins with carbon tape.

TGA analysis

The thermal characteristics of MCC, CNCs and CNC film were studied with a LabSys evo differential thermogravimetric analyzer (Setaram, France), in an argon atmosphere. The temperature range was 30 ± 5 – 700 ± 5 °C, with a heating rate of 10 ± 1 °C/min. The mass of the samples was approximately 20 ± 2 mg.

Results and discussion

The concentration of PAA obtained

According to the calculation based on formula 1 (above), the concentration of the PAA obtained was 12%.

Characterization of materials

Figure 2 shows the raw material and the product obtained in the present study. In Fig. 2a, the raw SFHs are of a pale color in the interior region and a black appearance on the outside region, due to the presence of phytomelanin pigment. Further, the unprocessed SFHs have a size range of 8–12 mm in length and 4–6 mm in width. Figure 2b shows an image of MCC, which, due to the presence of residual pigment, is gray in color, with a cotton-like fibrous appearance.

Determination of microcrystalline cellulose yield and quality

The results of MCC yield and quality obtained at different ratios of SFH:PAA via the organosolvent oxidation method are shown in Table 1 and Fig. 3. At a ratio of 1:16 g/mL the first noticeable increase in the activity of the delignification process occurs. At 1:20 g/mL, the pulp yield reaches a high level,

47.8±2%. Further increases in PAA raise the cellulose yield by only 0.04% (Table 1). Therefore, the ratio of 1:20 g/mL is considered the most effective and shall be used in further studies, taking into account the consumption of reagents. Finally, MCC obtained at the ratio of 1:20 g/mL was used in CNC synthesis.

In terms of quality analysis, the SFH:PAA ratio of 1:20 g/mL was found to produce the highest value of α -cellulose (72 ± 3%). The minimum content of residual lignin and hemicellulose was also observed at 1:20, resulting in 2.1±0.5% and 13.02±2%, respectively (Table 1). The moisture and ash content (SiO₂) of the MCC obtained (Table 1) did not differ significantly from previous studies (Ritesh et al. 2019). The unprocessed biomass of the annual plants used in the study showed a content of β -cellulose ranging from 30 to 60% and a content of residual lignin from 12 to 22%. Comparing these values to those of MCC, the effectiveness of the method of organosolvent oxidation in increasing the quantity of cellulose is clearly demonstrated. Of note is that oxidative-organosolvent technology allows extraction of MCC from SFHs under mild conditions and at high output without excessive pressure or temperature. In the process of obtaining MCC from SFHs, this delignification method was found to be quite effective (Table 1).

Surface morphology, particle size and suspension stability of MCC

The surface morphology of MCC is shown in Fig. 3. MCC fibers have an average length of 200–300 μ m and a width of 3.73–21.30 μ m, and a surface that is clean and relatively smooth. This indicates that cellulose microfibrils obtained from SFHs during organosolvent oxidation are separate, with limited quantities of hemicellulose and lignin.

The average particle size of MCC fibers was found to be 1971 ± 100 nm in length and 266 ± 35 nm in width (Fig. 4 and Table 2). Figure 5a shows an image of the freshly prepared MCC aqueous suspension and 5b shows an image of the MCC aqueous suspension after one month. Following a month, the MCC can be seen to fall out of suspension under the influence of gravity.

Preparation, surface morphology, particle size and suspension stability of CNC

Figure 6 is a diagram of CNC extraction from MCC using acid hydrolysis, and shows the resulting CNCs. The CNC yield from the MCC was 35 ± 1%. In a previous study (Chen et al. 2015), nanocellulose was obtained using acid hydrolysis from SFHs, and had a yield of 31.67%. Compared to that study, the present one yielded 3.33% more CNC volume.

In Fig. 7, the SEM microphotographs show that the surface of the CNC obtained using sulfuric acid hydrolysis consists of agglomerated fibrils. Acid hydrolysis breaks down the amorphous parts of the MCC and converts the microfibrils into nanofibrils. The process of hydrolysis significantly reduces the size of microcrystalline fibers, resulting in a length of 450 ± 50 and width of 50 ± 15 nm (Table 2). Furthermore, additional agglomeration of nanofibrils may be due to the effect of interfacial hydrogen bonding. Onkarappa et al. (2020) and Radakisnin et al. (2020) have shown that nanofibrils obtained through acid hydrolysis from various raw materials are agglomerated and achieve an average diameter of 50–150 nm. Thus, the CNC surface morphology obtained from SFHs did not differ from the CNCs obtained from other raw materials.

The average length of the CNCs reduced by 4 times to 450 ± 50 nm, as compared to the particle size of MCC, and the width shrunk by around 5 times to 50 ± 15 nm (Fig. 8 and Table 2). Figures 9a, b show that the CNC aqueous suspension remains unchanged after one month. A white homogeneous solution without any precipitation is shown in Fig. 9b, which indicates its stability. Figure 9a also shows the unimpeded passage of laser light through the CNC suspension. This is due to the Tyndall effect, which is caused by the impact of charges on the surface of cellulose nanoparticles (Zhan et al. 2018; Elanthikkal et al. 2010; Mohamed et al. 2015). In order to clarify the cause of the above effect, the zeta potentials of MCC and CNC aqueous suspensions were determined, and were found to be negative in both cases. The zeta potential value of the CNC suspension in 80 wt% phosphoric acid was -21.2 mV. The zeta potential results showed the formation of an electric charge between the shear plane of the final external layer and the bulk solution. This shows that during acid

hydrolysis negative charges accumulate on the CNC surface, leading to an increase in the zeta potential.

UV–vis analysis of CNCs and CNC film

Figure 10 shows that the layer of 18 ± 1 μm thick CNC film is both colorless and transparent. CNCs and CNC film were recorded in the ultraviolet spectrum at a wavelength of 200 to 1000 nm (Fig. 11). The spectra of the two samples did not show the absorption of the electron transitions of the $\pi\text{--}\pi^*$ (C=O) bond of the aromatic ring at a wavelength of 260–280 nm (Fig. 11a). This purity is explained by complete purification of lignin and hemicellulose (Lamia et al. 2009; Claudia et al. 2015), which can be clearly seen in the FTIR spectrum shown in Fig. 13.

The CNC film optical transmittance became smaller as the wavelength decreased, and the maximum absorption in the visible region was $50 \pm 1\%$ (Fig. 11b). The CNC film has high clarity and a good transparency. A study by Trifol et al. (2017) found that CNC film obtained from sisal fibers has good optical properties. Compared to the results of previous studies, the optical properties of the CNC film obtained here are generally better.

Morphological aspects of CNC film

The surface microstructure of CNC film is shown in Fig. 12. The surface of the CNC film appears homogeneous and consists of rod-shaped nanofibrils. Due to the shrinkage of fibers, the crystal is compacted and in rod form. In addition, the presence of a surface charge, caused by the sulfo groups, on the nanocrystallites has a positive effect on the homogeneity of the film surface (Martha et al. 2014; Trifol et al. 2017).

FT IR spectroscopy of MCC, CNCs and CNC film

Comparative FTIR spectra of the chemical structures of MCC, CNCs and CNC film obtained under the established optimal conditions (1:20 g/mL) are shown in Fig. 13. IR spectroscopy shows the absorption regions in all spectra: 655.9 cm^{-1} , at the C–OH bond due to out-of-plane bending (Zghari et al. 2018; Stefan et al. 2020); 891 cm^{-1} and 1153.6 cm^{-1} β - (1,4), caused by the glycoside C–O–C, an amorphous region (Zghari et al. 2018; Stefan et al. 2020); 1014.7 cm^{-1} and 1153.6 cm^{-1} high-intensity signals, from C–O

and C–C bonds in the aromatic ring and C–O in the pyranose ring; 1053.3 cm^{-1} , showing chronic oscillations of the C bond; 1253.9 cm^{-1} , 1307.9 cm^{-1} and 1365.8 cm^{-1} , due to the C–H bond; 1412.1 cm^{-1} , from the C–H₂ groups (Zghari et al. 2018; Stefan et al. 2020; Kacuráková et al. 2002; Kian et al. 2017; Haafiz et al. 2014); 1635.9 cm^{-1} , caused by the O–H in the water molecule sorbed from the air (Zghari et al. 2018); and, 2889.8 cm^{-1} and 3337.8 cm^{-1} , due to the CH and OH groups (Trifol et al. 2017; Kondo et al. 1996; Cao et al. 2004) (Fig. 13). In the MCC spectrum, 1516.2 cm^{-1} is associated with C=C in the aromatic ring of lignin (Sun et al. 2005), and 1724.6 cm^{-1} shows a chronic oscillation of the acetyl and ester group, C=O, in the hemicellulose molecule (Trifo et al. 2017). This confirms the accuracy of the numerical values of hemicellulose given in Table 1, and indicates the effective extraction of lignin and hemicellulose during the production of CNCs via acid hydrolysis. IR spectra show that the chemical structure of CNCs is similar to that of MCC, and that acid hydrolysis does not destroy the chemical structure of MCC (Djalal et al. 2014; Benyoussef et al. 2015). The result obtained is in good agreement with Kian et al. (2017). Finally, the chemical structure of CNC film shows no significant differences from the structure of CNCs themselves (Fig. 13).

X-ray diffractometry of MCC, CNCs and CNC film

In general, the crystallinity of cellulose is an important characteristic that determines its thermal and mechanical properties. Figure 14 shows a comparative X-ray diffractogram of MCC, CNCs and CNC film. A survey of the relevant literature was done to assess the crystallinity of cellulose (Podgorbunskikh et al. 2018; Mondragon et al. 2014). Four diffraction peaks are observed, equal to $2\theta = 15.6$ (1–10), 16.5 (110), 22.2 (200) and 34.5 (004), which demonstrate that the crystal structure of the molecule is characteristic of a two-chain monoclinic unit cell. They are the counterparts to the peaks of the cellulose I β pattern (French 2014). The diffractogram of the CNC film showed a loss of peak intensities of $2\theta = 15.60$ (1–10) and 16.50 (110), which may be due to higher oxygen ingress into the crystallite layers during air drying of the CNC film (Kazi et al. 2021). At the aforementioned ideal ratio of 1:20 g/mL, MCC has a CI of $72.9 \pm 4\%$, a CSL

at 2.9 ± 0.1 nm, and an average fiber particle size of 1971 ± 100 nm in length and 266 ± 35 nm in width (Table 2).

The CI content of the CNCs obtained via acid hydrolysis increased to $82 \pm 4\%$, and the CSL value decreased to 2.7 ± 0.1 nm. This demonstrates that during the chemical treatment, non-cellulose components are effectively removed from the amorphous part of the lignin, hemicellulose and cellulose, further increasing β -cellulose content (Martins et al. 2011). This is also evident from the results of SEM images of CNCs and CNC film (Figs. 7 and 12). The crystal structure of the film obtained from CNCs was not greatly changed in comparison with the CNCs themselves.

Thermo gravimetric analysis of MCC, CNCs and CNC film

Figure 15 is of the relative thermograms showing the thermal stability of MCC, CNCs and CNC film. The mass reduction of all samples can be divided into three stages. The first stage involves a decrease in mass in all samples, due to evaporation of water molecules at a temperature range of 35–125 °C (Voronova et al. 2015; Zhan et al. 2018). At the same time, MCC lost around 11% by weight, while the maximum reduction in the mass of CNCs and CNC film was approximately 6%, which is clearly evident from the XRD results (Fig. 14 and Table 2).

At the second stage, a significant loss of sample mass occurred in the temperature range of 200–358 °C. MCC, CNCs and CNC film lost 63%, 50% and 51% of their mass, respectively. The CNCs and CNC film lost a comparatively smaller amount of mass, which may be due to the high number of crystallites in the CNCs (Augusta et al. 2018). At this temperature range, cellulose is strongly depolymerized, while volatile components, such as CO, CO₂ and CH₄, are formed (Roman 2004). A sharp decrease in MCC mass is observed to start at a temperature of 254 °C, whereas the mass reduction of CNCs and CNC film begins at a temperature of 226 °C, with most decrease in the latter occurring in the range of 226–366 °C. The thermal stability of CNCs and CNC film was lower than that of MCC. This is due to the rapid degradation of the sulfate groups on the surface

of the CNCs (Roman et al. 2004; Kusmono et al. 2020). In the final stage, thermal decomposition of intermediate volatile products, such as levoglucosan, coke, hydrogen, ethylene, ethane and resin, occurs in the temperature range of 360–700 °C (Roman et al. 2004).

Conclusions

The present study has shown that an effective method for obtaining MCC from SFHs is conversion via the organosolvent oxidation method, with an ideal SFH to PAA ratio of 1:20 g/mL. The MCC quality indicators support this assertion, with β -cellulose at $72 \pm 3\%$, residual lignin at $2.1 \pm 0.5\%$, hemicellulose at $13.7 \pm 2\%$, humidity at $2.75 \pm 0.5\%$, and ash content (SiO₂) at $2.2 \pm 0.5\%$.

CNCs were synthesized at a yield equal to $35 \pm 1\%$ from MCC via sulfuric acid hydrolysis (60 wt%), which could later be made into CNC film using the previously outlined method. FTIR analysis of all products showed that their chemical structures are similar to each other. Analysis of average particle size showed that CNC crystals were several times smaller than MCC particles. Further, the average CI value increased from $72.9 \pm 4\%$ (MCC) to $82 \pm 4\%$ (CNCs) and CSL decreased from 2.9 ± 0.1 nm to 2.7 ± 0.1 nm, respectively.

The relative crystal structure of the CNC film was shown not to differ in any significant way from the original CNCs. Additionally, UV spectroscopy demonstrated that the dispersion of the CNCs in an aqueous medium was very high. Further, the Zeta potential was measured at -21.2 mV. Finally, the transmission coefficient of the CNC-film was equal to $50 \pm 1\%$.

The SEM results show that MCC fibers have a smooth surface, while the morphology of CNCs consists of agglomerated fibrils. The surface of the CNC-film shows homogeneous rod-like nanofibrils. All synthesized cellulose materials were shown to undergo degradation in the temperature range of 200–358 °C, and lose 51–63% of their mass.

The present study demonstrates that by adopting the modified organosolvent oxidation process, MCC can be easily extracted from SFHs, which can then

be further processed into nanocellulose. Hence, the present method can be employed successfully for the cost-effective production of nanocellulose. Moreover, the method is relatively environmentally friendly, highly efficient and an excellent protocol for the extraction of nanocellulose from SFHs.

Funding This study was conducted without any funding.

Declarations

Conflict of interest The authors declare that they have no conflicts of interest.

References

- Abdul Khalil HP, Davoudpour Y, Islam MN, Mustapha A, Sudesh K, Dungani R, Jawaid M (2014) Production and modification of nanofibrillated cellulose using various mechanical processes: a review. *Carbohydr Polym* 99:649–665. <https://doi.org/10.1016/j.carbpol.2013.08.069>
- Alemdar A, Sain S (2008) Bicomposites from wheat straw nanofibers: morphology, thermal and mechanical properties. *Compos Sci Technol* 68:557–565. <https://doi.org/10.1016/j.compscitech.2007.05.044>
- Alves JS, Reis KC, Menezes EG, Pereira FV, Pereira J (2015) Effect of cellulose nanocrystals and gelatin in corn starch plasticized films. *Carbohydr Polym* 115:215–222. <https://doi.org/10.1016/j.carbpol.2014.08.057>
- An VN, Nhan HT, Tap TD, Van T, Van T, Viet P (2020) Extraction of high crystalline nanocellulose from biorenewable sources of vietnamese agricultural wastes. *J Polym Environ* 28:1465–1474. <https://doi.org/10.1007/s10924-020-01695-x>
- Augusta I, de Jéssica P, Carlos MV, Andréia BH, Angelo M, Luciano AM (2018) From nano- to micrometer scale: the role of microwave-assisted acid and alkali pretreatments in the sugarcane biomass structure. *Biotechnol Biofuels* 11:73. <https://doi.org/10.1186/s13068-018-1071-6>
- Barbash VA, Yashchenko OV (2020) Preparation and application of nanocellulose from non-wood plants to improve the quality of paper and cardboard. *Appl Nanosci* 10:2705–2716. <https://doi.org/10.1007/s13204-019-01242-8>
- Belén M, Maite R, Saddys RL, Luis B, Rebeca B (2017) Effect of nanocellulose as a filler on biodegradable thermoplastic starch films from tuber, cereal and legume. *Carbohydr Polym* 157:1094–1104. <https://doi.org/10.1016/j.carbpol.2016.10.073>
- Benyoussif Y, Aboulhrouz S, El Achaby M, Cherkaoui O, Lallam A, El Bouchti M, Zahouily M (2015) Preparation and properties of bionanocomposite films reinforced with nanocellulose isolated from Moroccan alfa fibres. *Autex Res J* 15:164–172. <https://doi.org/10.1515/aut-2015-0011>
- Blaise LT, Mariko A, Jia QG, Maryam B, Tero T, Orlando JR (2017) Optical properties of self-assembled cellulose nanocrystals films suspended at planar-symmetrical interfaces. *Small* 13:1702084. <https://doi.org/10.1002/sml.201702084>
- Boerjan W, Ralph J, Baucher M (2003) Lignin biosynthesis. *Annu Rev Plant Biol* 54:519–546. <https://doi.org/10.1146/annurev.arplant.54.031902.134938>
- Bondeson D, Mathew A, Oksman K (2006) Optimization of the isolation of nanocrystals from microcrystalline cellulose by acid hydrolysis. *Cellulose* 13:171–180. <https://doi.org/10.1007/s10570-006-9061-4>
- Bongao HC, Gabatino RR, Arias A, Magdaluyo JR (2020) Micro/nanocellulose from waste Pili (*Canarium ovatum*) pulp as a potential anti-ageing ingredient for cosmetic formulations. *Mater Today* 22:275–280. <https://doi.org/10.1016/j.matpr.2019.08.117>
- Brown RM, Saxena IM (2000) Cellulose biosynthesis: a model for understanding the assembly of biopolymers. *Plant Physiol Biochem* 38:57–67. [https://doi.org/10.1016/S0981-9428\(00\)00168-6](https://doi.org/10.1016/S0981-9428(00)00168-6)
- Cao Y, Tan H (2004) Structural characterization of cellulose with enzymatic treatment. *J Mol Struct* 705:189–193. <https://doi.org/10.1016/j.molstruc.2004.07.010>
- Carrier M, Loppinet-Serani A, Denux D, Lasnier JM, Ham-Pichavant F, Cansell F, Aymonier C (2011) Thermogravimetric analysis as a new method to determine the lignocellulosic composition of biomass. *Biomass Bioenergy* 35:298–307. <https://doi.org/10.1016/j.biombioe.2010.08.067>
- Chen S, Tao HJ, Wang YJ, Ma ZS, Zhang LP (2015) Process optimization of nanocrystalline cellulose from sunflower seed hull and its characterization. *Nongye Gongcheng Xuebao/trans Chin Soc Agric Eng* 312:302–308. <https://doi.org/10.11975/j.issn.1002-6819.2015.15.041>
- Claudia DS, Juan SR, Markus RW, Bartlomiej G, Martin K, Yasser RB, Yamila G, Jani-Markus M, Alejandro RG, Jouni A, Clivia MS (2015) Optical and mechanical properties of nanofibrillated cellulose: towards a robust platform for nextgeneration green technologies. *Carbohydr Polym* 126:40–46. <https://doi.org/10.1016/j.carbpol.2015.03.032>
- Djalal T, André D, Kamel K, Riad B, Nicolas B (2014) Physico-chemical properties and thermal stability of microcrystalline cellulose isolated from Alfa fibres. *Carbohydr Polym* 104:223–230. <https://doi.org/10.1016/j.carbpol.2014.01.058>
- Dmytro Y, Anatoliy M (2021) Utilizing of sunflower ash in the wet conversion of phosphogypsum – a comparative study. *Environ Chall* 5:100241. <https://doi.org/10.1016/j.envc.2021.100241>
- Edgar CD, Gray DG (2001) Induced circular dichroism of chiral nematic cellulose films. *Cellulose* 8:5–12. <https://doi.org/10.1023/A:1016624330458>
- Elanthikkal S, Gopalakrishnanapanicker U, Varghese S, Guthrie JT (2010) Cellulose microfibrils produced from banana plant wastes: isolation and characterization. *Carbohydr Polym* 80:852–859. <https://doi.org/10.1016/j.carbpol.2009.12.043>
- French AD (2014) Idealized powder diffraction patterns for cellulose polymorphs. *Cellulose* 21:885–896. <https://doi.org/10.1007/s10570-013-0030-4>
- Gibson LJ, Ashby MF, Harley BA (2010) Cellular materials in nature and medicine. Cambridge University Press, Cambridge

- Gray DG (2016) Recent advances in chiral nematic structure and iridescent color of cellulose nanocrystal films. *Nanomaterials* 6:213. <https://doi.org/10.3390/nano6110213>
- Haafiz KM, Hassan A, Zakaria Z, Inuwa IM (2014) Isolation and characterization of cellulose nanowhiskers from oil palm biomass microcrystalline cellulose. *Carbohydr Polym* 103:119–125. <https://doi.org/10.1016/j.carbpol.2013.11.055>
- Hamawand I, Seneweera S, Kumarasinghe P, Bundschuh J (2020) Nanoparticle technology for separation of cellulose, hemicellulose and lignin nanoparticles from lignocellulose biomass: a short review. *Nano-Struct Nano-Objects* 24:100601. <https://doi.org/10.1016/j.nanos.2020.100601>
- Harkov V, Tuncev D, Kuznecov M (2018) Thermochemical processing of sunflower husk. *Vestnik Kazan State Agrarian Univ* 13:130–134. https://doi.org/10.12737/article_5c3de39d111083.70940804
- Israel AU, Obot IB, Umoren SA, Mkpene V, Asuquo JE (2008) Production of cellulosic polymers from agricultural wastes. *E-J Chem* 5:81–85. <https://doi.org/10.1155/2008/436356>
- Jayaraj AP, Ravindranath AD, Sarma US (2014) Nanocellulose from diseased coconut wood biomass. *CORD* 30:1–10. <https://doi.org/10.37833/cord.v30i1.80>
- Jean LW, Jean MP, Olivier B (2010) Cellulose science and technology. Chemistry. EPFL Press, Berlin, Fundamental Sciences
- Kacuráková M, Smith AC, Gidley MJ, Wilson RH (2002) Molecular interactions in bacterial cellulose Composites studied by 1D FT-IR and dynamic 2D FT-IR spectroscopy. *Carbohydr Res* 337:1145–1153. [https://doi.org/10.1016/S0008-6215\(02\)00102-7](https://doi.org/10.1016/S0008-6215(02)00102-7)
- Kazi MZ, Vincenzo C, Marcelo AS, Julien S, Saffron JB, Towhidul I, Reda MF, Janet LS, Karen JE (2021) Microstructural, thermal, crystallization, and water absorption properties of films prepared from never-dried and freeze-dried cellulose nanocrystals. *Macromol Mater Eng* 306:1–12. <https://doi.org/10.1002/mame.202000462>
- Khan Z, Ahmad S, Al-Sweih N, Chandy R (2005) Sunflower seed husk agar: a new medium for the differentiation of *Candida dubliniensis* from *Candida albicans*. *Indian J Med Microbiol* 23:182–185. <https://doi.org/10.4103/0255-0857.16605>
- Khusid SB, Gneush AN, Nesterenko EE (2015) Sunflower husk as a source of functional feed additives. *Polythematic Online Scientific Journal of Kuban State Agrarian University* 107:142–155. <http://ej.kubagro.ru/2015/03/pdf/08.pdf>
- Kian LK, Jawaid M, Ariffin H, Allothman OY (2017) Isolation and characterization of microcrystalline cellulose from roselle fibers. *Int J Biol Macromol* 103:931–940. <https://doi.org/10.1016/j.ijbiomac.2017.05.135>
- Kim J, Jayaramudu T, Zhai L, Kim HC, Agumba DO (2020) Preparation of cellulose nanocrystal-reinforced physical hydrogels for actuator application. *Curr Comput-Aided Drug Des* 10:969. <https://doi.org/10.3390/cryst10110969>
- Kondo T, Sawatari C (1996) A Fourier transform infra-red spectroscopic analysis of the character of hydrogen bonds in amorphous cellulose. *Polymer* 37:393–399. [https://doi.org/10.1016/0032-3861\(96\)82908-9](https://doi.org/10.1016/0032-3861(96)82908-9)
- Kunaver M, Anžlovar A, Žagar E (2016) The fast and effective isolation of nanocellulose from selected cellulosic feedstocks. *Carbohydr Polym* 148:251–258. <https://doi.org/10.1016/j.carbpol.2016.04.076>
- Kusmono FLR, Muhammad WW, Mochammad NI (2020) Preparation and characterization of cellulose nanocrystal extracted from ramie fibers by sulfuric acid hydrolysis. *Heliyon* 6:e05486. <https://doi.org/10.1016/j.heliyon.2020.e05486>
- Kvien I, Tanem BS, Oksman K (2005) Characterization of cellulose whiskers and their nanocomposites by atomic force and electron microscopy. *Biomacromol* 6:3160–3165. <https://doi.org/10.1021/bm050479t>
- Lamia T, Nour HM, Hatem BO, Hassen B, Sadok R (2009) Partial characterization of extracellular polysaccharides produced by cyanobacterium *Arthrospira platensis*. *Biotechnol Bioprocess Eng* 14:27–31. <https://doi.org/10.1007/s12257-008-0102-8>
- Lin G, Na F, Siyuan L, Shuyu Z, Zhen L, Jin H (2019) Assembly-induced emission of cellulose nanocrystals for hiding information particle and particle systems characterization. *Part Part Syst Charact*. <https://doi.org/10.1002/ppsc.201800412>
- Ling Z, Tuo W, Mohamadamin M, Michael SC, Cheng HN, Xue K, Markus B, Antje P, Thomas R, Holly K, Christopher DD, Sunghyun N, Vincent JE, Seong HK, Feng X, French AD (2019) Effects of ball milling on the structure of cotton cellulose. *Cellulose* 26:305–328. <https://doi.org/10.1007/s10570-018-02230-x>
- Lwako MK, Joseph KO, Baptist KJ (2013) A Review on pulp manufacture from non wood plant materials. *Int J Chem Eng* 4:144–148. <https://doi.org/10.7763/IJCEA.2013.V4.281>
- Martha AH, Mathew PA, Kristiina O (2014) Gas permeability and selectivity of cellulose nanocrystals films (layers) deposited by spin coating. *Carbohydr Polym* 112:494–501. <https://doi.org/10.1016/j.carbpol.2014.06.036>
- Martins AM, Eliângela MT, Ana CC, Mariselda F, Luiz HM (2011) Extraction and characterization of cellulose whiskers from commercial cotton fibers. *J Mater Sci* 46:7858–7864. <https://doi.org/10.1007/s10853-011-5767-2>
- Mohamed MA, Salleh WN, Jaafar J, Asric SE, Ismailab AF (2015) Physicochemical properties of “green” nanocrystalline cellulose isolated from recycled newspaper. *RSC Adv* 5:29842–29849. <https://doi.org/10.1039/C4RA17020B>
- Mondragon G, Fernandes S, Retegi A, Peña C, Algar I, Eceiza A, Arbelaiz A (2014) A common strategy to extracting cellulose nanoentities from different plants. *Ind Crops Prod* 55:140–148. <https://doi.org/10.1016/j.indcrop.2014.02.014>
- Oksman K, Mathew A, Bondeson D, Kvien I (2006) Manufacturing process of cellulose whiskers/poly(lactic acid) nanocomposites. *Compos Sci Technol* 66:2776–2784. <https://doi.org/10.1016/j.compscitech.2006.03.002>
- Onkarappa HS, Prakash GK, Pujar GH, Rajith Kumar CR, Latha MS, Virupaxappa SB (2020) Hevea brasiliensis mediated synthesis of nanocellulose: effect of preparation methods on morphology and properties. *Int J Biol Macromol* 160:1021–1028. <https://doi.org/10.1016/j.ijbiomac.2020.05.188>

- Ovcharov SN, Dolgikh OG (2010) Method of obtaining carbon adsorbent from sunflower husk. Russian Federation Patent 2395336
- Perea-Moreno MA, Manzano-Agugliaro F, Perea-Moreno AJ (2018) Sustainable energy based on sunflower seed husk boiler for residential buildings. *Sustainability* 10:3407. <https://doi.org/10.3390/su10103407>
- Podgorbunskikh EM, Bychkov AL, Bulina NV, Lomovskii OI (2018) Disordering of the crystal structure of cellulose under mechanical activation. *J Struct Chem* 59:201–208. <https://doi.org/10.1134/S0022476618010328>
- Quaranta N, Pelozo G, Cesari A, Cristóbal A (2016) Characterization of sunflower husk ashes and feasibility analysis of their incorporation in soil and clay mixtures for ceramics. *WIT Trans Ecol Environ* 203:13–23. <https://doi.org/10.2495/EID160021>
- Radakisnin R, Abdul Majid MS, Jamir MR, Jawaid M, Sultan MT, Mat Tahir MF (2020) Structural, morphological and thermal properties of cellulose nanofibers from Napier fiber (*Pennisetum purpureum*). *Materials* 13:4125. <https://doi.org/10.3390/ma13184125>
- Rambabu N, Panthapulakkal S, Sain M, Dalai AK (2016) Production of nanocellulose fibers from pinecone biomass: Evaluation and optimization of chemical and mechanical treatment conditions on mechanical properties of nanocellulose films. *Ind Crops Prod* 3:746–754. <https://doi.org/10.1016/j.indcrop.2015.11.083>
- Ritesh K, Sanju K, Shivani SS, Bhuvneshwar R, Rakesh K, Sidhharth S, Gulshan K (2019) A simple approach for the isolation of cellulose nanofibers from banana fibers. *Mater Res Express* 6:105601. <https://doi.org/10.1088/2053-1591/ab3511>
- Roman M, William TW (2004) Effect of sulfate groups from sulfuric acid hydrolysis on the thermal degradation behavior of bacterial cellulose. *Biomacromol* 5:1671–1677. <https://doi.org/10.1021/bm034519+>
- Rosana M, Francisco V, Monica E (2016) Cellulose nanocrystals from forest residues as reinforcing agents for composites: a study from macro-to nano-dimensions. *Carbohydr Polym* 139:139–149. <https://doi.org/10.1016/j.carbpol.2015.12.020>
- Sá RM, Miranda SC, José NM (2015) Preparation and characterization of nanowhiskers cellulose from fiber arrowroot (*Maranta arundinacea*). *Mater Res* 18:225–229. <https://doi.org/10.1590/1516-1439.366214>
- Saleh ME, El-Refaey AA, Mahmoud AH (2016) Effectiveness of sunflower seed husk biochar for removing copper ions from wastewater: a comparative study. *Soil Water Res* 11:53–63. <https://doi.org/10.17221/274/2014-SWR>
- Sintu R, Dan Y, Enrique GD, Esther GW (2019) Progress and opportunities in the characterization of cellulose – an important regulator of cell wall growth and mechanics. *Front Plant Sci* 9:1894. <https://doi.org/10.3389/fpls.2018.01894>
- Song JH, Murphy RJ, Narayan R, Davies GB (2009) Biodegradable and compostable alternatives to conventional plastics. *Phil Trans R Soc B* 364:2127–2139. <https://doi.org/10.1098/rstb.2008.0289>
- Stefan C, Masek A (2020) IR study on cellulose with the varied moisture contents: insight into the supramolecular structure. *Materials* 13:4573. <https://doi.org/10.3390/ma13204573>
- Sumira R, Himjyoti D (2020) Characterization of nanocellulose extracted from short, medium and long grain rice husks. *Ind Crops Prod* 154:112627. <https://doi.org/10.1016/j.indcrop.2020.112627>
- Sun C, Lu J (2019) Effect of sectional polymerization process on Tunable twist structure liquid crystal filters. *Curr Comput-Aided Drug Des* 9:268. <https://doi.org/10.3390/cryst9050268>
- Sun XF, Xu F, Sun RC, Fowler P, Baird MS (2005) Characteristics of degraded cellulose obtained from steam-exploded wheat straw. *Carbohydr Res* 340:97–106. <https://doi.org/10.1016/j.carres.2004.10.022>
- Tomasz K, Ryszard C, Małgorzata U (2021) High efficiency of the removal process of Pb(II) and Cu(II) ions with the use of fly ash from incineration of sunflower and wood waste using the CFBC technology. *Energies* 14:1771. <https://doi.org/10.3390/en14061771>
- Trifol J, Sillard C, Plackett D, Szabo P, Bras J, Daugaard AE (2017) Chemically extracted nanocellulose from sisal fibres by a simple and industrially relevant process. *Cellulose* 24:107–118. <https://doi.org/10.1007/s10570-016-1097-5>
- Voronova MI, Surov OV, Guseinov SS, Barannikov VP, Zakharov AG (2015) Thermal stability of polyvinyl alcohol/nanocrystalline cellulose composites. *Carbohydr Polym* 130:440–447. <https://doi.org/10.1016/j.carbpol.2015.05.032>
- Vurasco AV, Driker BN (2014) Cellulose from annual plants. LAP LAMBERT Academic Publishing, Germany, Organo-oxidizing solvent cooking
- Yandan C, Qiaomei W, Biao H, Mingjie H, Xiaolin A (2015) Isolation and characteristics of cellulose and nanocellulose from lotus leaf stalk agro-wastes. *BioResources* 10:684–696. <https://doi.org/10.15376/biores.10.1.684-696>
- Zajemska M, Urbańczyk P, Poskart A, Dariusz U, Henryk R, Dorota M, Grzegorz G, Tomasz W (2017) The impact of co-firing sunflower husk pellets with coal in a boiler on the chemical composition of flue gas. *E3S Web Conf* 14:02021. <https://doi.org/10.1051/e3sconf/20171402021>
- Zghari B, Hajji L, Boukir A (2018) Effect of moist and dry heat weathering conditions on cellulose degradation of historical manuscripts exposed to accelerated ageing: 13C NMR and FTIR spectroscopy as a non-invasive monitoring approach. *J Mater Environ Sci* 9:641–654. <https://doi.org/10.26872/jmes.2018.9.2.71>
- Zhan HW, Zheng JY, Jin TZ, Meng H, Qiong J, Shuiping L, Yuanye M, Manqing L, Sen L (2018) Isolation and characterization of cellulose nanocrystals from pueraria root residue. *Int J Biol Macromol* 129:1081–1089. <https://doi.org/10.1016/j.ijbiomac.2018.07.055>

Publisher's Note Springer Nature remains neutral with regard to jurisdictional claims in published maps and institutional affiliations.